Quantum Mechanics Applications Using the Time Dependent Schrödinger Equation in COMSOL

A. J. Kalinowski*[1]
[1]Consultant
*Corresponding author: East Lyme CT 06333, kalinoaj@aol.com

Abstract: COMSOL is used for obtaining the quantum mechanics wave function Ψ(x,y,z,t) as a solution to the *time dependent* Schrödinger equation. The probability determination of a particle being at a spatial point can be treated by a) the "matrix mechanics formulation" or b) the "Schrödinger wave function formulation". The latter approach is used herein, because it involves solving field partial differential equations, thus is adaptable to COMSOL.

Keywords: Quantum Mechanics, Time Dependent Schrödinger Equation.

1. Introduction

The purpose of this paper is to illustrate the use of COMSOL for obtaining the quantum mechanics wave function Ψ(x,y,z,t) (represents *matter waves*) as a solution to the *time dependent* Schrödinger equation. In quantum mechanics, solutions for the probability of a particle being at a particular point in space are usually treated through a) the "matrix mechanics formulation" originated by Werner Heisenberg or b) the "Schrödinger wave function formulation" originated by Erwin Schrödinger. The latter approach is the one used herein, mainly because it involves solving field partial differential equations, and therefore is adaptable to COMSOL. Once having determined the wave function Ψ(x,y,z,t), it can be normalized and then used to compute the probability of a particle being in a specific zone within the computational spatial field under consideration. Two example problems are solved to illustrate the procedure for solving Schrödinger's equation with COMSOL. The first is a simple 2-D bar used for testing the FEM accuracy of the *time dependent* wave propagation of Ψ. At atomic scales, the location in space of entities such as electrons, have dual behavioral characteristics, where they act both as a particle and a wave [1]. The second example illustrates this wave like behavior by employing a barrier model with two embedded slits. When stream of particles (e.g., electrons) impinges on the two slit barrier, experiments reveal that the location of the particles hitting a screen located on the barrier's back side appear in bands [2]. Depending on the screen location, the maximum number of hits in a band does not necessarily line up with the location of the slits as expected if the impinging electrons were acting according to regular Newtonian particle trajectories. A COMSOL solution to the time dependent Schrödinger's equation predicts a similar result, where the magnitude of the complex wave function squared, (i.e., *probability density* ≡ $|\Psi|^2$), also appears in similar bands, where the $\int |\Psi|^2 \, dA$ over finite area zone ΔA, is directly related to the probability of a particle being located within ΔA.

2. Governing Equations

The governing equation for the behavior of a particle of mass *m* in the presence of a potential field V, is represented by the *time dependent* quantum mechanics Schrödinger equation (with wave function Ψ(x,y,z,t) as the primary dependent variable) and is given by [1]:

$$\nabla^2\Psi + i\underbrace{\frac{2m}{\hbar}}_{a}\frac{\partial\Psi}{\partial t} - \frac{2mi}{\hbar^2}V\Psi = 0 \qquad (1)$$

with $\hbar = h/(8\pi)$, where *h* is Plank's constant, and $i = \sqrt{(-1)}$. In the rest of the paper we consider only non-relativistic free particles, where V=0.

3. Method

The governing Eq.(1) is solved explicitly in the time domain by the FEM method in COMSOL, subject to time harmonic drivers which vary as exp(-iωt). Schrödinger's equation has been solved using COMSOL in the past, but for *time independent* forms of Eq.(1). COMSOL has a "built in Schrödinger Equation Interface", however it is for eigenfunction *time independent* forms and therefore not applicable here. The

COMSOL users manual and previous COMSOL conference archives, also have several examples of the *time independent* application, however there appears to be none that treat the *time dependent* form of the solution. In this paper, the transient study type is employed within the General Form PDE section of the Equations Based Modeling. An incident plane wave of the form Ψ= ΨoExp(ikx-iωt), with Ψo=1.0 , is generated by driving the left end face of the model with Ψ= ΨoExp(-iωt). Further, an absorbing boundary condition is developed in order to terminate the mesh at the extreme right end of the model and is implemented via the flux/source settings using the boundary absorption /impedance term.

4. Theory

Wave solutions of Eq.(1) in the *x* direction are sought of the form:

$$\Psi = \widehat{\Psi}(x)\exp(-i\omega t) \qquad (2)$$

Equation (2) is substituted into Eq.(1) and solving the resulting second order o.d.e. yields:

$$\widehat{\Psi}(x) = \Psi_0 \exp(ikx) \quad where \ k = \pm\sqrt{a\omega} \qquad (3)$$

where the plus sign is used for waves traveling in the +x direction and Ψ_0 is an arbitrary constant amplitude. Similarly, a wave traveling in an arbitrary unit vector direction $\boldsymbol{\eta}$ (bold variables within the text denote vectors hereafter) is given by:

$$\Psi(x,y,t) = \Psi_0 \exp(i\vec{k}\bullet\vec{r} - i\omega t) \qquad (4)$$

where wave number vector **k** and position vector **r** are given by:

$$\vec{k} = k\vec{\eta} \qquad \vec{\eta} = \eta_x\vec{e}_x + \eta_y\vec{e}_y \qquad (5)$$

$$\vec{r} = x\vec{e}_x + y\vec{e}_y \qquad \vec{n} = n_x\vec{e}_x + n_y\vec{e}_y \qquad (6)$$

with $(\mathbf{e_x}, \mathbf{e_y})$ denoting conventional Cartesian coordinate unit vectors (**i**, **j**). When the wave impinges upon a domain boundary surface (having a unit outward normal ***n*** to the surface), a wave absorbing boundary condition is considered later and the effect of $\boldsymbol{\eta}$ not being inline with ***n*** is discussed.

The phase velocity of the traveling wave is given by Eq.(7) and since the phase velocity depends on frequency, these traveling waves are dispersive. This is in contrast to the classical non-dispersive wave equation (e.g., linear acoustics) where the phase velocity is $v_\varphi=\omega/k=c$, with c a constant constructed from the medium bulk modulus and density .

$$v_\phi \equiv \frac{\omega}{k} = \sqrt{\frac{\omega}{a}} = \sqrt{\frac{\hbar\omega}{2m}} \qquad (7)$$

4.1 Model Driver

An incident plane wave of the form Ψ= ΨoExp(ikx-iωt), with constant Ψo, is implemented by driving the left end face of the model with:

$$\Psi(0,t) = \widetilde{\Psi}_0 \exp(-i\omega t) \qquad (8)$$

The k-ω relation Eq.(3) is dispersive, therefore we do not want to introduce any unwanted frequency components (beside the drive ω) during the startup of the wave generation. In order to avoid the suddenly applied real part of the driver at t=0, the amplitude in Eq.(8) is exponentially increased from a small fraction of Ψo (i.e., ε), to 1.0 over time span t_c:

$$\widetilde{\Psi}_0 = \Psi_0 \exp(\beta(t-t_c)) \quad 0 \le t < t_c \qquad (9)$$
$$\widetilde{\Psi}_0 = \Psi_0 \quad t_c \le t \le \infty$$
$$\beta = -\frac{\log_e(\epsilon)}{t_c}$$

The values of Ψo=1.0, t_c =2T (2 time cycles) and ε =.05 were used in the examples to follow, where T corresponds to one cycle (T=2π/ω).

4.2 Absorbing Boundary Condition

When the boundary is driven with Eq.(8), the outward traveling going wave will eventually reach a boundary surface of the FEM model. A simple plane wave impedance type boundary condition is used at that surface of the form:

$$\vec{\nabla}(\Psi(x,y,t))\bullet\vec{n} = ik\Psi(x,y,t) \qquad (10)$$

where ***n*** is the unit outward normal to the surface. This type of boundary condition is usually used for steady state (*time independent*) problems; however, when the response frequency content contains a dominant driver ω content (e.g., Figure 2a inset), and if the field traveling wave is close to being normal to the surface, then this condition works adequately.

Plane Waves: For example, if a plane wave traveling in the direction $\boldsymbol{\eta}$ impinges on a surface with unit normal $\boldsymbol{n}$, the fulfillment of Eq. (10) is tested by substituting Eqs.(4), (5) and (6) into boundary condition Eq.(10) to get:

$$ik\Psi(x,y,t)\underbrace{\{n_x\eta_x+n_y\eta_y\}}_{\cos(\phi)}=?\,ik\Psi(x,y,t) \qquad (11)$$
$$\vec{n}\bullet\vec{\eta}=n_x\eta_x+n_y\eta_y=\underbrace{|\vec{n}||\vec{\eta}|}_{1.0}\cos(\phi)=\cos(\phi)$$

Thus Eq.(11) suggest that making the replacement of $k\rightarrow k\cos(\varphi)$ on the r.h.s. in Eq. (10), would improve the quality of the absorber but would require knowing the $\boldsymbol{\eta}$ direction of the plane wave. A graphical illustration of the $\boldsymbol{\eta}$, $\boldsymbol{n}$ and φ are illustrated in Figure 1 (wave fronts emerging from slits are actually curved), where for the "base case" geometry depicted, $\cos(\varphi)$ varies from 1.0 at the poles to a worse case value of $\sqrt{(1-(S/2R)^2)}=0.92$ opposite the slit (see Figure 5 for S and R definitions). The worse case value is 0.96 for the bigger Figure 5d model since R is 7/5 times larger.

Cylindrical Waves: Consider a cylindrical wave originating from the origin at point A in Figure 1.We seek solutions of the form:

$$\Psi(r,t)=\widehat{\Psi}(r)\exp(-i\omega t) \qquad (12)$$

and upon substituting Eq.(12) into Eq.(13) (i.e. the cylindrical coordinate form of Eq.(1))

$$\frac{\partial^2\Psi}{\partial r^2}+\frac{1}{r}\frac{\partial\Psi}{\partial r}+ia\frac{\partial\Psi}{\partial t}=0 \qquad (13)$$

one obtains a Bessel differential equation

$$\frac{d^2\widehat{\Psi}}{dr^2}+\frac{1}{r}\frac{d\widehat{\Psi}}{dr}+\underbrace{a\omega^2}_{k^2}\widehat{\Psi}=0 \qquad (14)$$

with solution given by:

$$\widehat{\Psi}(r)=\widetilde{A}H_0^{(1)}(kr)\approx\underbrace{\widetilde{A}\sqrt{2/\pi}\exp(-i\pi/4)}_{\Psi_0}\frac{\exp(ikr)}{\sqrt{kr}}$$
$$\Psi(r,t)=\Psi_0\frac{\exp(ikr-i\omega t)}{\sqrt{kr}} \qquad (15)$$

The $H_0^{(1)}$ is a zero order Hankel function of the first kind and is approximated by the above exponential form for large $kr>>1$. Therefore Equation (15) behaves like a decaying plane wave far enough away from the origin (this is where the absorbing boundary condition will be used). The satisfaction of the absorbing boundary condition Eq.(10), is checked by first noting:

$$r=\sqrt{x^2+y^2}\quad \vec{n}\equiv\vec{e}_r=\frac{x\vec{e}_x+y\vec{e}_y}{\sqrt{x^2+y^2}} \qquad (16)$$
$$\vec{\nabla}(\Psi)=\frac{\partial\Psi}{\partial x}\vec{e}_x+\frac{\partial\Psi}{\partial y}\vec{e}_y$$

and then substituting second of Eqs.(15) and Eqs.(16) into Eq.(10) to obtain:

$$ik\Psi(x,y,t)\underbrace{\left(\frac{x^2+y^2}{r^2}\right)}_{1}\underbrace{\left(1+\frac{i}{2kr}\right)}_{\approx1;\,kr>>1}=?\,ik\Psi(x,y,t)$$

The Eq.(10) is nearly satisfied, where the second term in parentheses is close to 1.0 for large kr arguments. For example problems considered later, $kr=10\pi$ at the outer mesh boundary, therefore $1/(2kr)=1/(20\pi)=.0159$ and therefore the second term in parentheses is 1+ 0.0159i .

4.3 Probability Computation

The wave function Ψ(x,y,t) can be used to compute the probability of a particle being in a particular area zone of space for 2-D models. However the *as is* wave function coming out of the FEM solution has to be normalized so that probability of a particle being in the *total* spatial domain of the problem description is 1.0 . The normalized wave function Ψ_n is obtained by first multiplying the unnormalized wave function Ψ by a yet to be dermined normalization factor denoted by Λ [4], i.e.,

$$\Psi_n(x,y,t)=\Lambda\Psi(x,y,t) \qquad (17)$$

Next the normalized probability density is integrated over the total spatial domain A_T (the zone where it is possible for the particle to be present), and then set equal to 1.0, thus

$$\iint_{A_T}|\Psi_n(x,y,t)|^2\,dA=1 \qquad (18)$$

Equation (17) is substituted into (18) and solving for Λ^2 gives Eq.(19).

The probability P_X of a particle being inside some sub area zone A_X within the total area A_T is then given by Eq.(20). The evaluation of Λ is difficult because the full field of Ψ(x,y,t) is not known beyond the artificial absorbing boundary.

Instead of P_X, the relative probability between

$$\Lambda^2 = 1/\iint_{A_T} |\Psi(x,y,t)|^2 dA \qquad (19)$$

$$P_X = \Lambda^2 \iint_{A_X} |\Psi(x,y,t)|^2 dA \qquad (20)$$

two neighboring zones is desired. Later we consider two area zones A_X=A_M, and A_X=A_U which correspond to one mid zone opposite the slit and the other upper zone above the slit. The relative probability ratio $R_{U/M}$ is defined by :

$$R_{U/M} = \frac{P_U}{P_M} = \frac{\Lambda^2 \iint_{A_U} |\Psi(x,y,t)|^2 dA}{\Lambda^2 \iint_{A_M} |\Psi(x,y,t)|^2 dA} \qquad (21)$$

where now the normalization factor Λ^2 cancels out and therefore is not needed for the $R_{U/M}$ relative computation. For example if $R_{U/M}$ >1, these means that it is more probable to have a particle located just to the side of the slit than directly in line with the slit, inferring diffraction .

5. Numerical Model

The primary problem solved herein is the 2 D field response to an incident plane wave $\Psi_i(x,y,t)$ function passing down a wave guide and then passing through two slits as shown in the upper

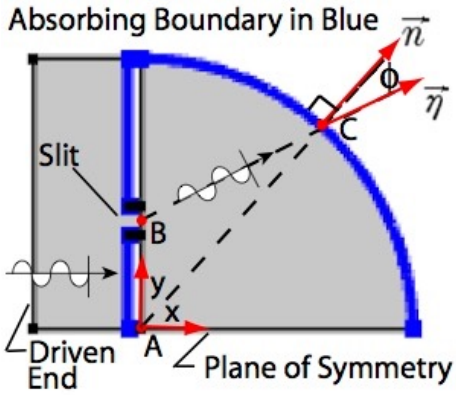

Figure 1. Upper Half FEM Model.

half of the two slit FEM model of Figure 1. Only half of the full two slit problem needs to be modeled because of an existing plane of symmetry at cut y=0. For the presentation of results, the full model (i.e., both upper and lower half are displayed using mirroring options). The example problems were all run using the "General Form PDE", with a "Time Dependent" study selection. The PDE Eq.(1) parameter of a=1.7268 s/cm^2 is used, with incident wave parameters of f=3.2953x10^7 Hz , Ψo=1.0, and tc =2/f in driver Eqs.(8) and (9) .

5.1 Boundary and Initial Conditions

Boundary Conditions:

Rigid boundary condition $\partial\Psi/\partial y$ =0 is used on the horizontal walls of the front end wave guide, on the slit tunnel walls, and on the plane of symmetry. Rigid boundary condition $\partial\Psi/\partial x$ =0 is used on the back side vertical wall separating the incident wave region and the transmitted side region. An absorbing boundary condition given by Eq.(10) is used on the surfaces shown in blue in Figure 1. The incident side vertical wall is made absorbing so that back reflections off this wall do not travel back to the drive surface. Equation (10) is implimentated using the *Flux/ Source* setting with COMSOL input parameters g=0 on the *boundary flux* term and *q=ik* on the *boundary absorption/impedance* term. The incident side vertical wall is parallel to the incoming wave front, therefore no cos(φ) correction would be needed. As shown in Figure 1, the slit is not at the origin of the circular boundary arc, therefore cylindrical waves (which start to look like decaying planar waves away from the slit), will not impinge exactly normal to the surface, and therefore there will be some absorption error introduced (like in Eq.(11)) which will introduce some small error depending on the size of φ. The FEM solutions are terminated in time before this error has any significant effect on the field solution and construction of interference patterns. This is an advantage of solving the problem in the time domain rather than as a steady state problem where the absorbers have to work over all time.

Initial Condition:

The PDE is first order in time thus, there is only one initial condition, namely that of $\Psi(x,y,0+)$=0.

5.2 Model Length and Time Size

Time and length quantities are very small at the atomic level. Therefore in the presentation of results , length quantities are given as a multiple of the incident traveling wave length $\lambda=2\pi/k$ and time is given as a multiple of the incident wave period $T=2\pi/\omega$. Therefore non-dimensional independent variables of $\chi_1=x/\lambda$, $\chi_2=y/\lambda$, and $\tau=t/T$ are used to plot results. Although not used

to generate the results presented herein, one could substitute these normalized variables into the free particle form of Eq.(1) to obtain $\partial^2\Psi/\partial\chi_1^2 + \partial^2\Psi/\partial\chi_2^2 + i2\pi\,\partial\Psi/\partial\tau = 0$, and then work with this non dimensional PDE where model sizes and time scales would be nice size numbers. The harmonic part of the end driver would then be proportional to exp(-i$2\pi\tau$).

The base case model shown in Figure 1 has a waveguide inlet length of 2λ (including the small slit length), where the radius of the backside chamber of R=5λ. The slit aperture opening (width) is W = $\lambda/2$ and the pitch (centerline to centerline of the slits) is S = 4λ . Variations on these parameters are considered in the results.

6. Results

A simple waveguide verification model is first solved, followed by the base case double slit model with additional variations on basic model parameters.These models are solved using the base case parameters given in section 5.0 .

6.1 WaveGuide Validation

The purpose of this example is to have an independent cross check on the COMSOL solution for the type of *time dependent* Schrödinger equations considered in this paper. The model (driven with Eq.(8)) is a variation on the front end of the wave guide Figure 1 example, except at the termination right end of the model there is no slit and the entire back boundary is terminated with Eq.(10) . The model (see Figure 2c inset) is of length L=2λ and width L/10 (the response is really 1-D so the width could be made narrower than the base case inlet, where 2-D elements are used to simulate what is employed in the base case two slit model).

An independent "exact solution" to this same problem is obtained by using Laplace transforms. The solution is exact up until we need to take the inverse Laplace transform. At that point there does not appear to be an exact inversion and numerical inverse algorithms are employed. First take the Laplace transform, £[ ], of the 1-D (free particle form, *V=0*) of Eq.(1) with respect to *t*, where the transformed *t*

$$\frac{d^2\psi(x,s)}{dx^2} + ias\psi(x,s) - ia\Psi(x,0+) = 0 \quad (22)$$

variable is the conventional *s* parameter and the transformed wave function variable is denoted by lower case ψ(x,s). This o.d.e. (with int. cond. Ψ (x,0+)=0) has a solution given by Eq.(23).

The arbitrary constants C_1 and C_2 are solved by substituting Eqs.(23) into the Laplace

$$\psi(x,s) = C_1\exp(\alpha x) + C_2\exp(-\alpha x) \quad (23)$$
$$\alpha = (i-1)\sqrt{\frac{as}{2}}$$

transform of the boundary conditions given by Eqs.(24), giving two linear algebraic equations for C_1 and C_2. Equations (24) contains s, therefore C_1 and C_2 will explicitly depend on s. Finally, the solved $C_1(s)$ and $C_2(s)$ are inserted

$$\psi(0,s) = \mathcal{L}\left(\overline{\Psi}_0(t)\exp(-i\omega t)\right) \quad (24)$$
$$\frac{\partial\psi(L,s)}{\partial x} = ik\psi(L,s)$$

into Eq.(23) and then inverse Laplace transformed to get to get the final solution:

$$\Psi(x,t) = \mathcal{L}^{-1}\left[C_1(s)\exp(\alpha x) + C_2(s)\exp(-\alpha x)\right] \quad (25)$$

Until now all the expressions, with the help of symbolic programming, are analytical in form. Thus the argument inside £$^{-1}$[ ] of Eq.(25) is explicitly known in terms of s, however analytically evaluating the inverse Laplace transform is extremely difficult, and numerical techniques [3] are used instead to obtain the last phase of the solution. It is labeled as an "exact solution", but actually it is a quasi exact solution.

The model end driver (i.e., Eq.(8)) used in all the FEM runs is shown in Figure 2a for Ψ vs t/T at x/λ =0 (the shape of the driver's Fourier transform frequency content amplitude, | Ƒ(Ψ) | vs ω, is shown in the inset, where the dominant spike is at the drive frequency). The FEM driver and the Laplace transform driver are essentially the same except COMSOL uses a small *S* shaped smoothing rise time zone over a time span of 0.1T. Thus the FEM startup is from zero instead of from εΨo.

There is good agreement between the exact solution vs the FEM solution in Figure 2c for the complex Ψ vs x/λ at τ=t/T=1.5 as the solution gradually builds, heading towards the desired ΨoExp(ikx-iωt). The Figure 2d plot shows the solution at a later time of t/T=4.0, where at this point the desired unit amplitude for Ψo and the peak to peak wavelength Δx/λ=1 is reached. This also illustrates the absorbing boundary condition at the end of the bar is working since no reflections are coming back. Figure 2b illustrates the response vs τ=t/T and shows how the response has progressed to a fixed observer at located at x/λ = 1.

6.2 Two Slit Base Case Solution

In Figure 3, a sequence of three time snapshots is illustrated in sub Figures 3a) $\tau=t/T=3.0$, 3b) $\tau=4.5$ and 3c) $\tau=6.0$. The real part of Ψ is plotted in order to give a better idea of how the diffraction is being set up as time evolves. The

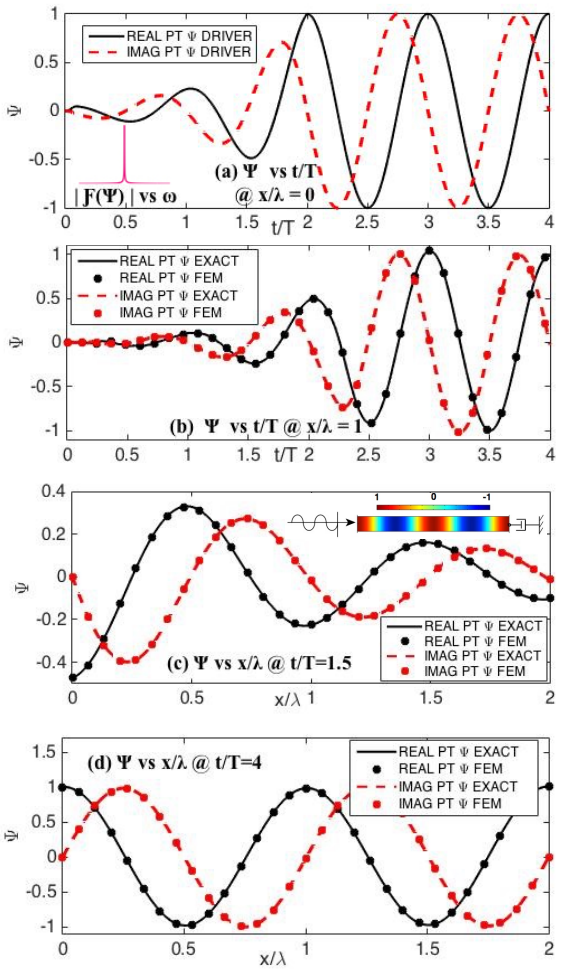

Figure 2. Waveguide FEM-Exact Comparison

last sub Figure 3d is also at $\tau=6.0$, however here $|\Psi|^2$ is plotted and a banded interference pattern evolves of the type that are observed experimentally [2]. A plot of $|\Psi|^2$ vs vertical coordinate y/λ at cut $x/\lambda=1.88$ given in Figure 4a and 4b (for the base case model $R=5\lambda$, and for a corresponding bigger $R=7\lambda$ model), show the bands more clearly. The location of the slice is shown by the red dashed line in Figure 3d and 5d. The location of the centerline of the two slits are shown by the horizontal dashed lines in Figure 4. The value of $|\Psi|^2$ is lower directly opposite the slit as say compared to values either directly above or below the slit, thus illustrating the wavelike diffraction of the wave function.

The probability of a particle being in one of the four probability zones of size $\Delta A=\lambda/4 \times \lambda/4$ is addressed, where the right side of the box shape zone is located at $x/\lambda=1.88$ which corresponds to the Figure 3d red dashed line. This is

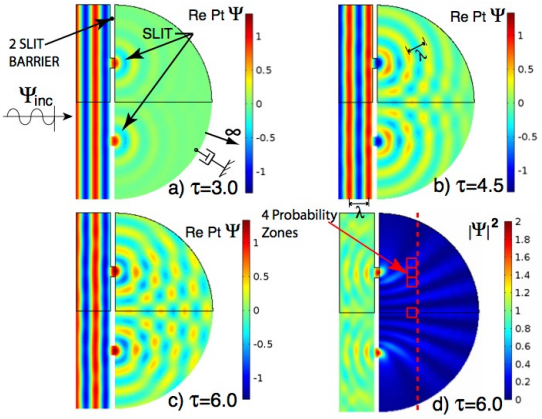

Figure 3. Base Case Two Slit Solution At Fixed Times

accomplished by evaluating $\int|\Psi|^2$ dA over each of the four probability zones shown in Figure 3d where the 4 red boxes are referred to as Upper, Mid, Lower and Plane of Symmetry. The mid

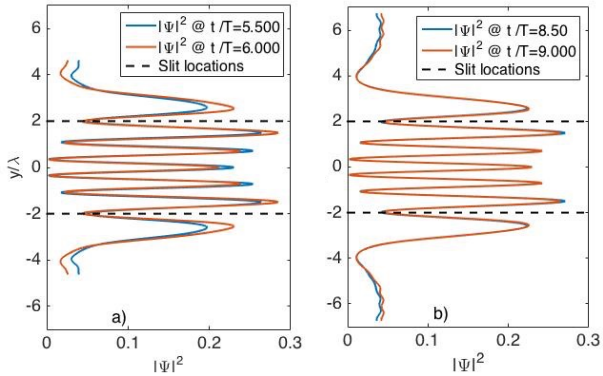

Figure 4. Section Cut, $|\Psi|^2$ vs y/λ @ $x/\lambda=1.88$: a) Base Case Model $R=5\lambda$, b) Big Model $R=7\lambda$

zone is located in line with the slit and it is therefore of interest to compute the probability of being in this "in-line mid zone" relative to neighboring zones. Upon applying Eq.(21) (for the probability ratio) to the computed field, it is observed that it is $R_{U/M}=1.74$ times more probable that a particle is found in the upper zone than in mid zone; $R_{L/M}=1.57$ times more probable that a particle is found in the lower zone than in mid zone , and $R_{PS/M}=.925$ times

less probable that a particle is found in the plane of symmetry zone than in mid zone. Placing these 4 probability zones at other locations, say farther out at a value of x/λ=2.87, results in the opposite situation where there is a greater probability the particle is in the mid zone, than either above or below it.

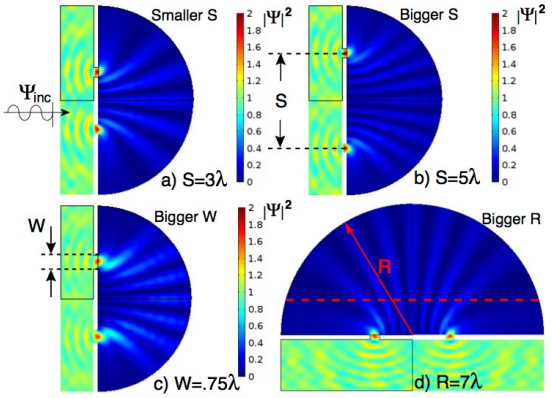

Figure 5. Sensitivity to Slit Pitch S, Aperture W and Model Size R

Lastly, for a given ω driver frequency, Eq.(3) gives the wave number k (and hence wave length sized by λ=2π/k) of the incident plane wave. This is the k used in boundary condition Eq.(10) for all model absorbing surfaces. This true length λ (e.g., drawn to scale) is superimposed on the peak to peak response on the incident side as shown in Figure 3b and thus good alinement is illustrated. A portion the plane wave has passed through the slit, and emerged on the back side as a cylindrical traveling wave. The spatial wave length still appears to be approximately λ as shown by the true length λ marker superimposed on the back side peak to peak curved wave response in Figure 3b where again good alinement is illustrated. This implies the outer boundary absorber sized by k=2π/λ does an adequate job.

6.3 Base Case Variations

The sensitivity of the solutions to the slit pitch S, aperture W and Model outer radius R is illustrated in Figure 5 where comparisons are made between the base case result in Figure 3d and those in Figure 5. The base case S= 4λ, has 8 dark blue minimum bands, but for smaller pitch S= 3λ, there are 6 bands and for bigger pitch S= 5λ, there are 10 bands. Regarding aperture variation, the bigger opening W= .75λ still has 8 minimum bands but they are less sharp than the W= .5λ base case. Finally the effect of model size on the base case is considered by increasing the base case model radius of R= 5λ to a bigger R= 7λ value. The big model size of Figure 5d (rotated 90 degrees to fit in the Figure) and base case size 5c are shown to the same scale so that a relative size visual illustration of the bigger model is achieved. The big model inlet wave guide is L=3λ compared to 2λ in the base case model. The first and eighth minimum bands show up more clearly in the bigger model, but overall comparing the Figure 3d base case and Figure 5d big model, the results are very similar, therefore indicating the model size of the base case is adequate. The big model has run a longer time (9T vs 6T), therefore upon comparing Figures 4a and 4b, the bigger model is closer to reaching a steady state condition (the two curves plotted per graph are for two neighboring times separated by 1/2 period in time), where the 4b pair of curves overlay closer than the 4a pair.

7. Conclusions

COMSOL can be used to solve the Schrödinger Equation in the time domain, using the General Form PDE implementation. The agreement between the exact vs FEM solutions for simple 2-D bar examples with absorbing boundary conditions to terminate infinite domains, was shown to be very good. Solutions to more complex problems like the incident plane wave upon a two slit barrier, produced diffraction patterns showing bands of null zones due to wave destructive interference. These null zones are not unlike the ones observed experimentally when a steady stream of electrons impinge upon a two slit barrier. The evaluation of the COMSOL solution for the probability of a particle location, showed that depending on the standoff distance from the back side of the barrier, it could be more likely to have the particle located off to the side of the slit projection, than in line with the slit projection. This diffraction interference illustrates the wave like behavior of particles at the atomic scale.

8. References

1. Leonard. Susskind,et al., “Quantum Mechanics”, Basic Books New York, 2014.

2. Kenneth W. Ford, “101 Quantum Questions”, Harvard University Press, Cambridge Ma, 2012.

3. Peter P. Valkó, P et al., “Gaver Meth. of Num. Laplace Transform Inversion”, Comp. & Math. with Appl. , (2002).

4. David McMahon,“Quantium Mechanics Demystified”, McGraw Hill NewYork, Second Edition, 2013, Page 26.